Electronic Supplementary Material (ESI) for Physical Chemistry Chemical Physics
This journal is © The Owner Societies 2012

Barrierless photoisomerisation of the "simplest cyanine": joining computational and femtosecond optical spectroscopies to trace the full reaction path

— Supporting Information —

Alexander Weigel[a], Matthias Pfaffe[a], Mohsen Sajadi[a], Rainer Mahrwald[a], Roberto Improta[b], Vincenzo Barone[c], Dario Polli[d], Giulio Cerullo[d], Nikolaus P. Ernsting[a*], Fabrizio Santoro[e*]

[a] *Department of Chemistry, Humboldt-Universität zu Berlin, Brook-Taylor-Strasse 2, 12489 Berlin, Germany*

[b] *CNR--Consiglio Nazionale delle Ricerche, Istituto di Biostrutture e Bioimmagini (IBB-CNR), Via Mezzocannone 16, 80134 Napoli*

[c] *Scuola Normale Superiore, piazza dei Cavalieri 7, 56126 Pisa, Italy*

[d] *IFN-CNR, Dipartimento di Fisica, Politecnico di Milano, p.zza Leonardo da Vinci 32, 20133 Milano, Italy*

[e] *CNR--Consiglio Nazionale delle Ricerche, Istituto di Chimica dei Composti OrganoMetallici (ICCOM-CNR), UOS di Pisa, Area della Ricerca, Via G. Moruzzi 1, I-56124 Pisa, Italy*

e-mail: fabrizio.santoro@iccom.cnr.it, nernst@chemie.hu-berlin.de

1. Synthesis of 1,1`-diethyl-2,2`-pyridocyanine iodide (1122-P)

1.1 General scheme

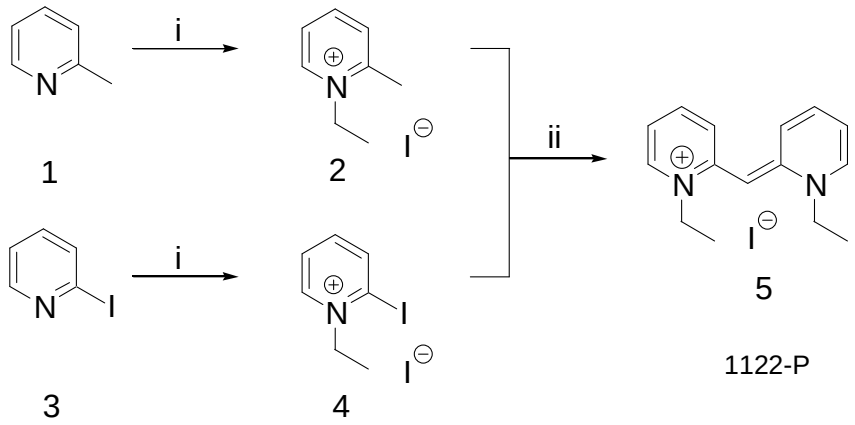

Scheme S1: Synthesis of 1,1`-diethyl-2,2`-pyridocyanine iodide (1122-P). *i* EtI, Δ; *ii* *n*-propanol, Et_3N.

The synthesis was accomplished by the following reaction sequence. α-Picoline **1** and 2-iodopyridine **3** were converted to the quaternary salts (**2**, **4**) by refluxing in the presence of ethyl iodide.[1,2] The quaternary salts **2** and **4** were refluxed in *n*-propanol with triethylamin to obtain the dye 1,1`-diethyl-2,2`-pyridocyanine iodide **5** (1122-P).[3]

1.2 Experimental details

Chloroform and ethanol were distilled. *n*-Propanol was dried and stored over molecular sieve (4 Å). All other reagents were used as obtained from the supplier without further purification. Purification of products was accomplished by recrystallization in ethanol/diethyl ether or by flash chromatography with silica gel 60. Thin layer chromatography was carried out with Merck Silica Gel 60 F_{254} TLC plates. HRMS were measured with LTQ-FT.

α-Picoline ethyl iodide **2**[1]

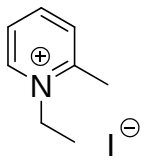

8.0 ml (81.0 mmol) α-picoline **1** and 19.5 ml (0.244 mol) ethyl iodide were refluxed for 2 hours. The remaining ethyl iodide was evaporated i. vac. and the yellow solid was recrystallised from ethanol under successive addition of diethyl ether. 16.3 g (81%) α-picoline ethyl iodide **2** were obtained as a white-yellow solid.

melting point: 130°C

HRMS: calc. for $[C_8H_{12}N]^+$: 122.0964 found: 122.0959

2-Iodopyridine ethyl iodide **4**[2]

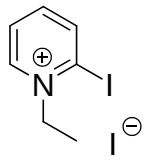

5.0 g (24.4 mmol) 2-iodopyridine **3** were dissolved in 6 ml (73.2 mmol) ethyl iodide. The mixture was refluxed for 8 hours. The remaining ethyl iodide was evaporated i. vac. and the white solid was recrystallised from ethanol under successive addition of diethyl ether. 5.1 g (58%) 2-iodopyridine ethyl iodide **4** were obtained as a white solid.

melting point: 159°C

HRMS: calc. for $[C_7H_9IN]^+$: 233.9774 found: 233.9765

1,1`-diethyl-2,2`-pyridocyanine iodide **5**[3]

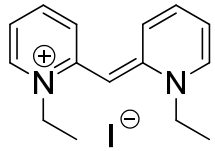

1.0 g (4.0 mmol) α-picoline ethyl iodide **2** and 1.45 g (4.0 mmol) 2-iodopyridine ethyl iodide **4** were dissolved in 20 ml *n*-propanol. 1.1 ml (8 mmol) triethylamine was added and the mixture refluxed for 45 minutes. The solvent was evaporated i. vac. and the residue purified by column chromatography (ethanol:chloroform 1:4). 1,1`-Diethyl-2,2`-pyridocyanine iodide **5** was obtained as a brown oil. Purification of compound **5** by recrystallization was unsuccessful.[3, 4] Nevertheless the obtained optical absorption spectra of 1122-P are in excellent agreement with the results in the literature.[3,5-7] Also we identified the product by high-resolution mass-spectroscopy.

HRMS: calc. for $[C_{15}H_{19}N_2]^+$: 227.1543 found: 227.1539

2. **Experimental results**

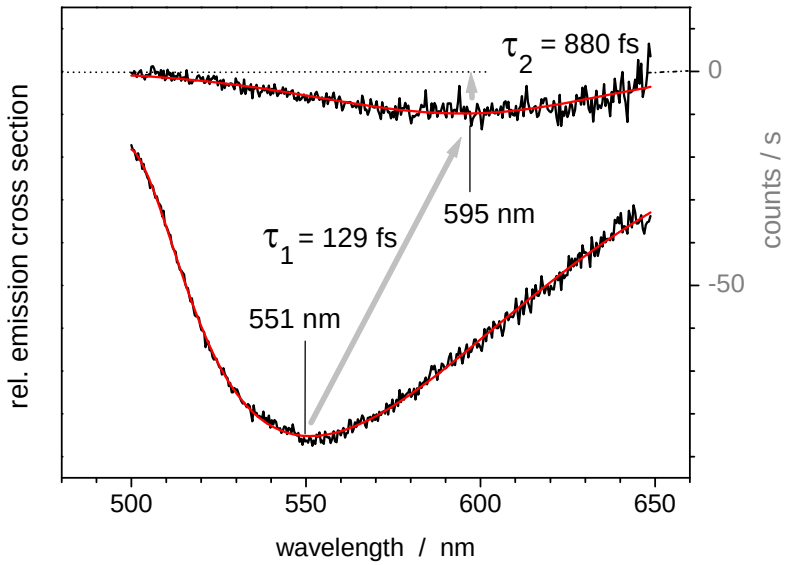

Fig. S1a Species-associated spectra of stimulated emission (from fluorescence as in **Fig. 3a**) for a kinetic sequence N* $\rightarrow$ O* $\rightarrow$ 0. *Black*: from global analysis, *red*: fit by lognormal functions. Note that the second spectrum is reliable for $\lambda \leq 620$ nm only (because the second harmonic of the gate pulse contributes a strongly fluctuating background around 650 nm). With the peak amplitudes, the intensity decay is approximated as $I_{FLUPS}(t) = 0.897\exp(-t/\tau_1) + 0.103\exp(-t/\tau_2)$. The average emission time becomes $\int_0^\infty I_{FLUPS}(t)\,dt = 0.206$ ps – the same, independently, as the first time constant for the transient absorption in **Fig. 2**. This allows us to insert the two fixed terms $\exp(-t/\tau_1)$ and $\exp(-t/\tau_2)$ into the global analysis of the TA data.

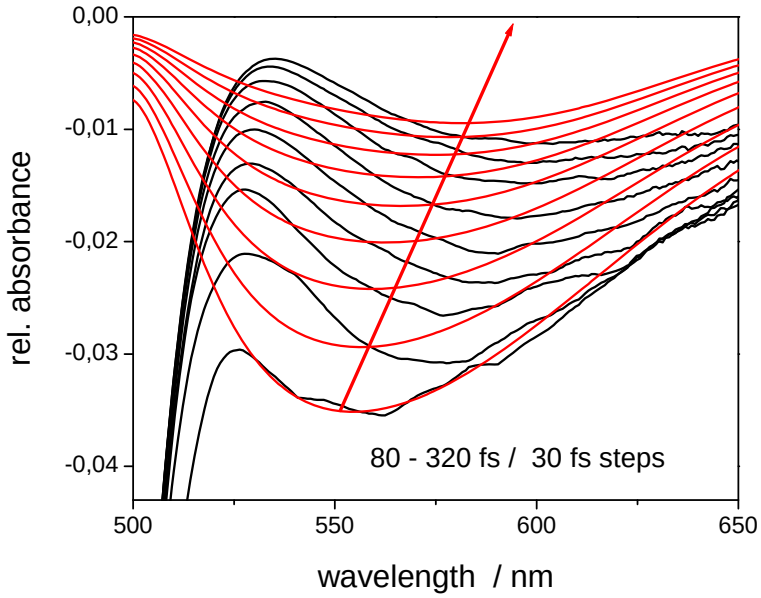

Fig. S1b Comparison of transient absorption signal (*black*, from excitation at 442 nm, taken from **Fig. 2a**) to stimulated emission (*red*, converted from the spontaneous fluorescence of **Fig. 4**). The amplitude of the latter has been scaled so that the peaks agree at 80 fs. The different TA behavior is explained by absorption from the excited state (ESA). Faint structure of stimulated emission at 80 fs (630 cm^{-1} spacing) is not considered significant.

3. Computational details

The description of solvent effects on excited-state properties through continuum models is usually performed in one of two limit time-regimes, referred to as nonequilibrium (*neq*) and equilibrium (*eq*).[8] In *neq* case, only solvent electronic polarization (fast solvent degrees of freedom) is in equilibrium with the excited state electronic density of the solute, whereas nuclear degrees of freedom (slow solvent degrees of freedom) remain equilibrated with the ground state electron density. On the contrary, in the *eq* regime it is assumed that both fast and slow degrees of freedom are equilibrated with the excited state electron density. In the PCM formalism the solvent reaction field in the *neq* regime depends on the dielectric constant at optical frequency $\varepsilon_{opt}=n^2$ where *n* is the solvent refractive index; for methanol $\varepsilon_{opt}=1.776$). PCM *eq* solvation is instead ruled by the static dielectric constant, $\varepsilon= 32.613$ for methanol. *Neq* solvation energies are more appropriate to simulate the vertical excitation and to discuss the fast part of the excited state dynamics (time after photoexcitation <200 fs), whereas the *eq* time regime can better model the excited state properties for the slower part of the excited state dynamics (time after excitation>1 ps).

In this work excited-state optimizations in methanol have been performed by using the "standard" LR (linear-response) implementation of PCM/TD-DFT, for which analytical gradients are available.[9] LR-PCM/TD-DFT excitation energies are computed without using the true excited state electron density. According to our previous studies LR model provides an accurate estimate of solvent effect on bright transitions and reliable excited state equilibrium geometries.[10-12] At variance, the State-Specific (SS) implementation of PCM/TD-DFT[13,14] is based on a fully variational formulation of the solvent effect on the excited state properties, and it solves a different effective Shroedinger equation for each electronic state of interest. SS implementation provides a more balanced description of solvent effects than LR-PCM, especially when dealing with transitions (like the CT ones) involving large changes of the electron density.[13,14]

The continuum solvent model adopted in this work cannot describe the intermolecular hydrogen bonds between methanol and 1122-P. By including explicit solvent molecules in calculations of a thiacyanine, we showed that these interactions should not affect the properties and photodynamics of the dye molecule seriously.[15] The multi-determinantal nature of the first excited state of cyanines, is a challenge for TD-DFT calculations.[16,17] In our case, it is comforting that PBE0 and B3LYP functionals provided an accurate description of the FC region of a thiacyanine[18,19] and a qualitatively correct picture of its isomerization path.[15] On the other hand, neither these functionals nor CAM-B3LYP are able to reproduce the effect of chain lengthening in cyanine derivatives.[20] This failure, however, should not be serious for a short-bridge cyanine like 1122-P.

4. Computational results

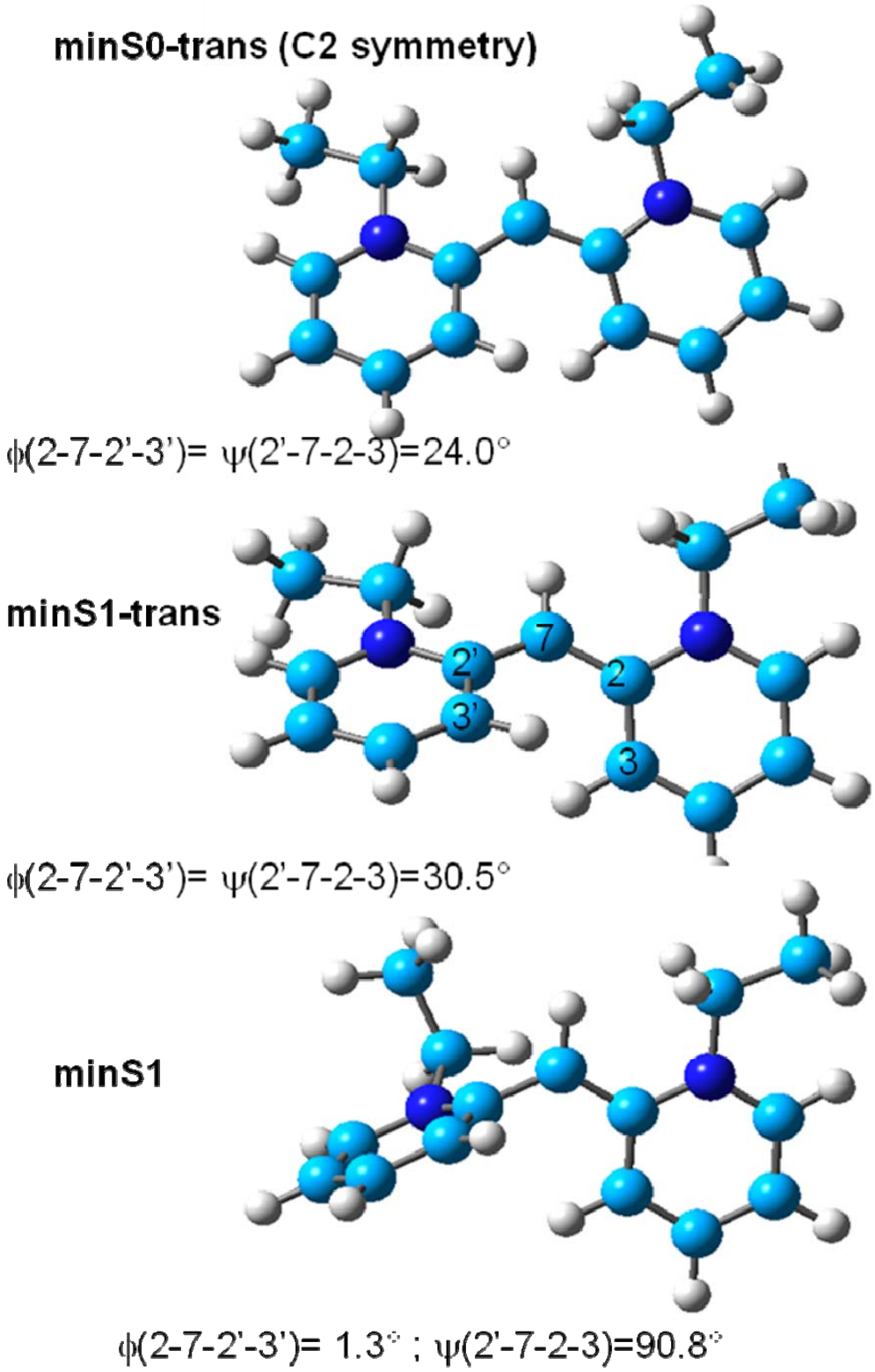

Fig. S2 Minima of 1122-P in methanol at the LR-PCM//CAM-B3LYP/6-31G(d) level of theory

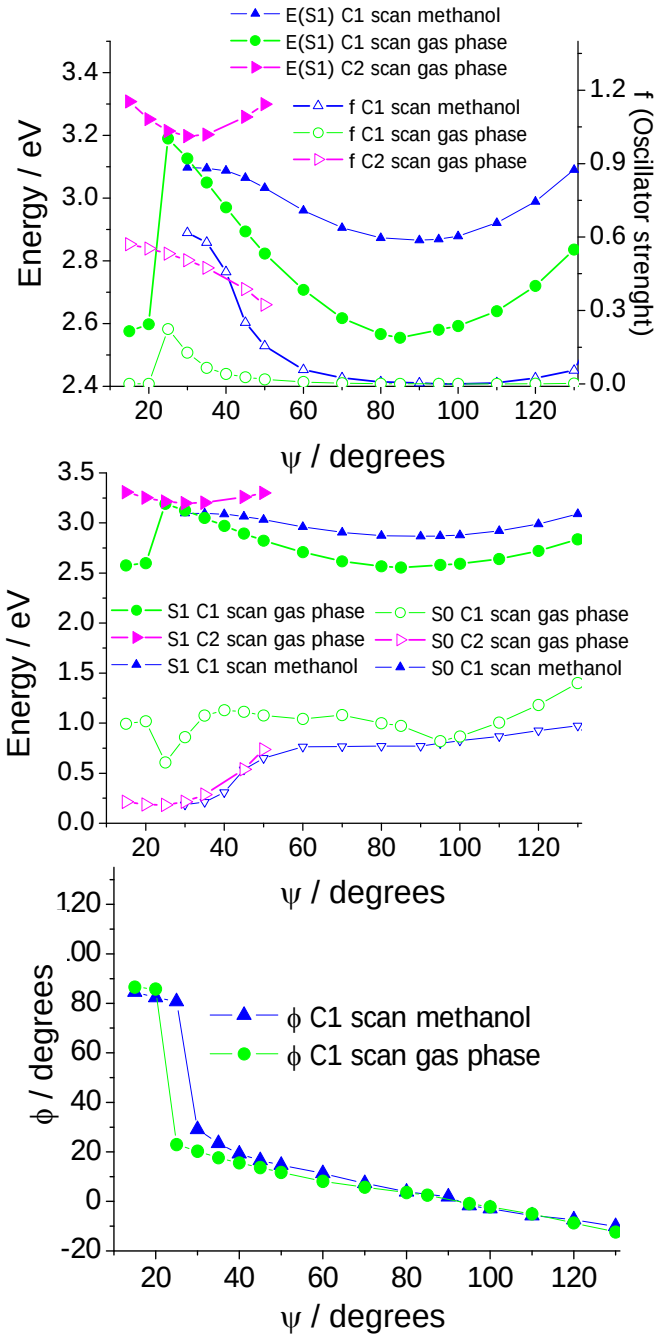

Fig. S3 CAM-B3LYP/6-31G(d) MEP of the S_1 PES of Me-1122-P in the gas-phase, and comparison with the C_1 results in methanol (LR results): a) S_1 energies and S_0/S_1 oscillator strength; b) S_0 and S_1 energies; c) ϕ values.

The results in gas phase, reported in **Fig. S3**, are similar to those obtained in methanol according to LR theory (and also given in **Fig. 9** in the main text). The only significant difference is seen in the C_1 MEP: one finds a stronger tendency to remove C_2 symmetry. While in methanol, the C_1 and C_2 MEPs remain very close in a narrow but well-defined range of ψ values (25–35°), in the gas phase they come close only at ψ=25°. Even for this value of ψ, the C_1 structure is slightly more stable. It

is also non-symmetric, as can be noticed clearly by the S_0 energy, which is much higher, and by the S_1/S_0 oscillator strength, which is much lower.

4. 1Comparison of *trans, cis* , and *d-cis* spectra according to FC|VG model

To achieve a robust and safe comparison of the spectra, not depending on discretional choices on how to obtain representative stationary points on the excited-state PES, we resorted to the simple FC|Vertical Gradient (VG) model. It assumes that the normal modes and frequencies of the final state (of the electronic transition) are equal to those of the initial state, and geometry displacements are estimated on the ground of the final state PES gradient at the equilibrium geometry of the initial state. Furthermore, Herzberg-Teller effects are neglected (after checking that they are very weak). By theory in this model, the first moment of the spectrum, i.e the average transition energy, coincides with the vertical transition energy.

Electronic results are reported in Table 1 and 2 that compare the CAM-B3LYP results already given in Table 1 and 2 in the main text with B3LYP ones. The corresponding spectra are given in **Fig. S4.**

Table 1 Energies (eV) of *trans*, *cis*, and *dcis* isomers on S_0 PES optimized in methanol by CAM-B3LYP and B3LYP, and *trans, dcis* and minS_1 stationary points on S_1 PES optimized in methanol at LR-PCM// CAM-B3LYP level. S_1 energies in nonequilibrium regime. When equilibrium regime values are given, they are reported in italics.

Structure	CAM-B3LYP				B3LYP			
	6-31G(d)		6-311+G(2d,2p)		6-31G(d)		6-311+G(2d,2p)	
	E (S0)	E(S1)	E(S0)	E (S1)	E (S0)	E(S1)	E(S0)	E (S1)
minS_0-*trans*	0.0	3.247	0.0	3.194	0.0	3.049	0.0	2.992
minS_1-*trans*	0.184	3.097 *2.885*						
minS_0-*cis*	0.176	3.401	0.181	3.349	0.181	3.203	0.184	3.144
minS_0-*dcis*	0.366	3.527	0.372	3.461	0.378	3.357	0.382	3.279
minS_1-*dcis*	0.831	*3.129*						
minS_1	0.776	2.867 *2.862*						

Table 2 *trans, cis* and *dcis* vertical excitation energies (eV) in nonequilibrium (*neq*) and equilibrium(*eq*) regimes

Structure	CAM-B3LYP							
	6-31G(d)				6-311+G(2d,2p)			
	LR *neq*	LR *eq*	SS *neq*	SS *eq*	LR *neq*	LR *eq*	SS *neq*	SS *eq*
minS_0-*trans*	3.247 (0.76)	3.019 (0.96)	3.353 (0.65)	3.335 (0.64)	3.194 (0.77)	2.962 (1.00)	3.290 (0.65)	3.267 (0.65)
minS_0-*cis*	3.225 (0.66)	3.018 (0.85)	3.317 (0.56)	3.286 (0.55)	3.168 (0.67)	2.958 (0.88)	3.248 (0.55)	3.194 (0.53)
minS_0-*dcis*	3.161 (0.593)	2.966 (0.79)	3.261 (0.49)	3.240 (0.49)	3.088 (0.58)	2.892 (0.80)	3.179 (0.48)	3.153 (0.47)
	B3LYP							
	6-31G(d)				6-311+G(2d,2p)			
	LR *neq*	LR *eq*	SS *neq*	SS *eq*	LR *neq*	LR *eq*	SS *neq*	SS *eq*
minS_0-*trans*	3.049 (0.55)	2.863 (0.80)	3.111 (0.42)	3.081 (0.41)	2.991 (0.56)	2.803 (0.83)	3.043 (0.41)	3.007 (0.40)
minS_0-*cis*	3.022 (0.50)	2.848 (0.72)	3.074 (0.37)	2.897 (0.245)	2.960 (0.49)	2.782 (0.74)		
minS_0-*dcis*	2.979 (0.45)	2.811 (0.67)	3.049 (0.34)	3.027 (0.34)	2.896 (0.43)	2.731 (0.67)	2.957 (0.32)	2.927 (0.31)

Oscillator strength in parentheses.

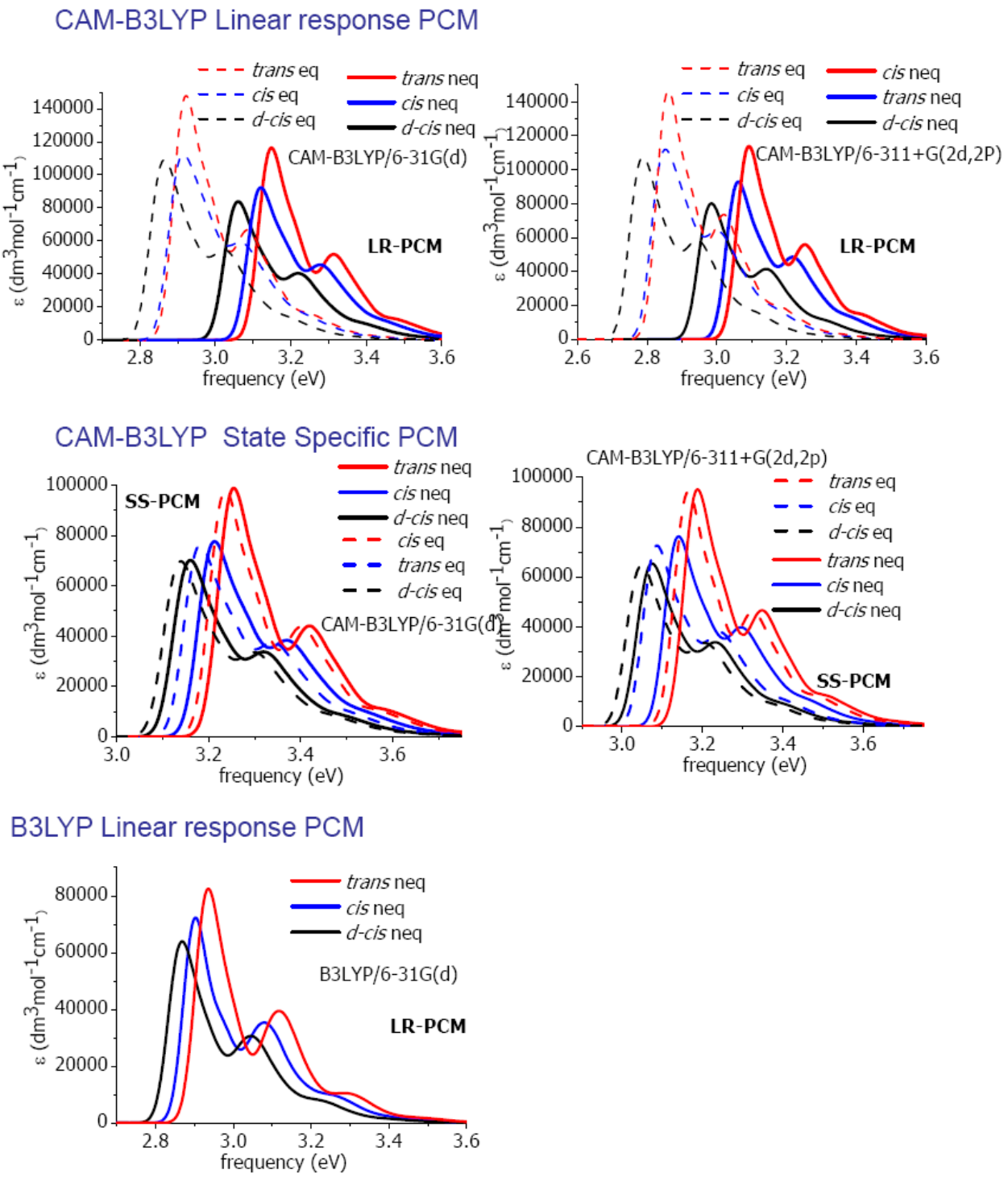

Fig. S4 Absorption spectra of the three isomers computed with the FC|VG model. The solvent is treated in the *equilibrium* (eq) and *nonequilibrium* (neq) regimes. Geometrical displacements were estimated from excited state energy gradients computed at the LR-PCM level, with the functional and basis set indicated. For SS spectra, excitation energies and transition dipole moments (but not energy gradients) were refined at the SS-PCM level. When two sets of data (dashed and solid lines) are given, the dashed lines report *eq* spectra and solid lines *neq* spectra.

4. 2 Assignments of Raman bands.

The assignment of Raman bands gives rises to interesting speculations. For the *trans* species, the strongest peaks (535, 640, 1305, 1340, 1665 cm^{-1}) are all related to symmetric motions of the two pyrido rings (modes 18, 23, 52, 54, 69, sketched in **Fig S6**), which describe the motion between the two symmetric minS_0-*trans* and minS_1-*trans* structures. To the contrary, for the *cis* species, the main bands calculated at 1230 and 1350 cm^{-1} correspond to vibrations with a strong component from bending of the central CH bond, coupled with ring motions. One may speculate that bands involving such CH bending are also responsible for the low-frequency peaks of the multiplet in the 1200-1300 cm^{-1} region, observed for *trans* species but not reproduced by calculations. Actually, according to the latter, modes involving this bending do exist for *trans* but they are dark to vRR (at VG level) since they remove the C_2 symmetry. Their observation in experiment suggests either a fast overcoming of the C_2 barrier along the MEP, or else the operation of the second C_1 path competitive with the one depicted in **Fig 7a,** that does not pass through minS_1-*trans*. Moreover, the higher-frequency mode has a localized character, showing a stronger contribution of displacements in the pyridine ring whose C-CH_3 bond points in the opposite direction with respect to the central C_7-H bond (the right ring in **Fig. 6,** top left). Therefore these modes are related to the asymmetrization of the two pyrido rings which eventually leads to the minS_1 structure. As such their nature is quite different from the modes of the calculated *trans* spectrum in the same frequency region.

RR activity in the low-frequency region 30-400 cm^{-1} is instructive as well. The long-time transient signal of *cis* species shows bands in this region which are significantly more intense and broader than those of the *trans* isomer. This feature is qualitatively captured by the VG simulation and can be attributed to the fact that, while the S_1 PES in the *trans* isomer region shows a plateau along ψ and ϕ dihedrals, and therefore no strong acceleration along twisting modes, no such plateau exists in the *cis* region and the system is immediately accelerated toward the global minimum structure minS_1.

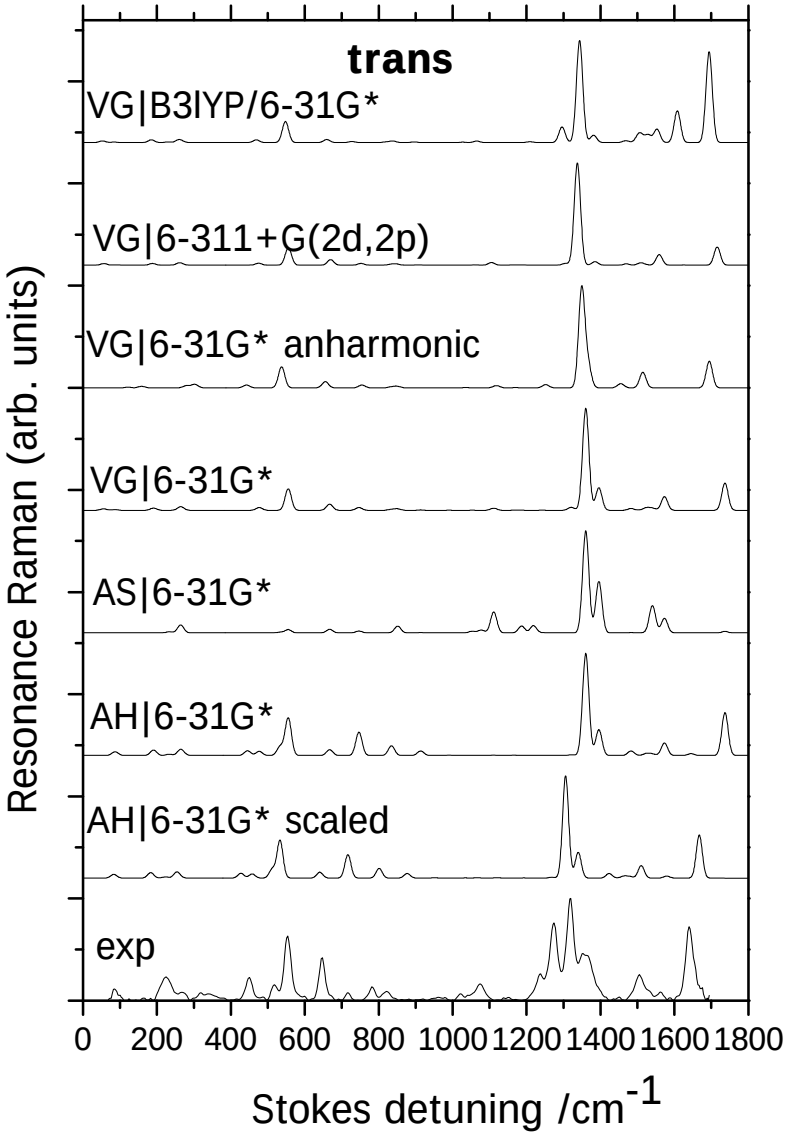

Fig. S5 Franck-Condon vibrational Raman spectra of the *trans* isomer of Me-1122-P, upon $S_0 \rightarrow S_1$ resonance. They were computed with different models and at different level of electronic theory. In the AH model the transition polarizability tensor is computed explicitly, taking into account Duschinsky rotation. The VG and AS models assume the same normal modes and frequencies for S_0 and S_1. They predict relative vRR intensities from the S_1 gradient (computed explicitly at the ground equilibrium geometry, VG, or estimated from the displacements obtained by S_1 geometry optimization, AS). When not stated differently, the CAM-B3LYP functional was used. "Scaled" indicates that calculated harmonic CAM-B3LYP/6-31G* frequencies have been multiplied by 0.96. Both anharmonic corrections and frequency scaling were applied by simply shifting the bands (leaving intensities unaffected).

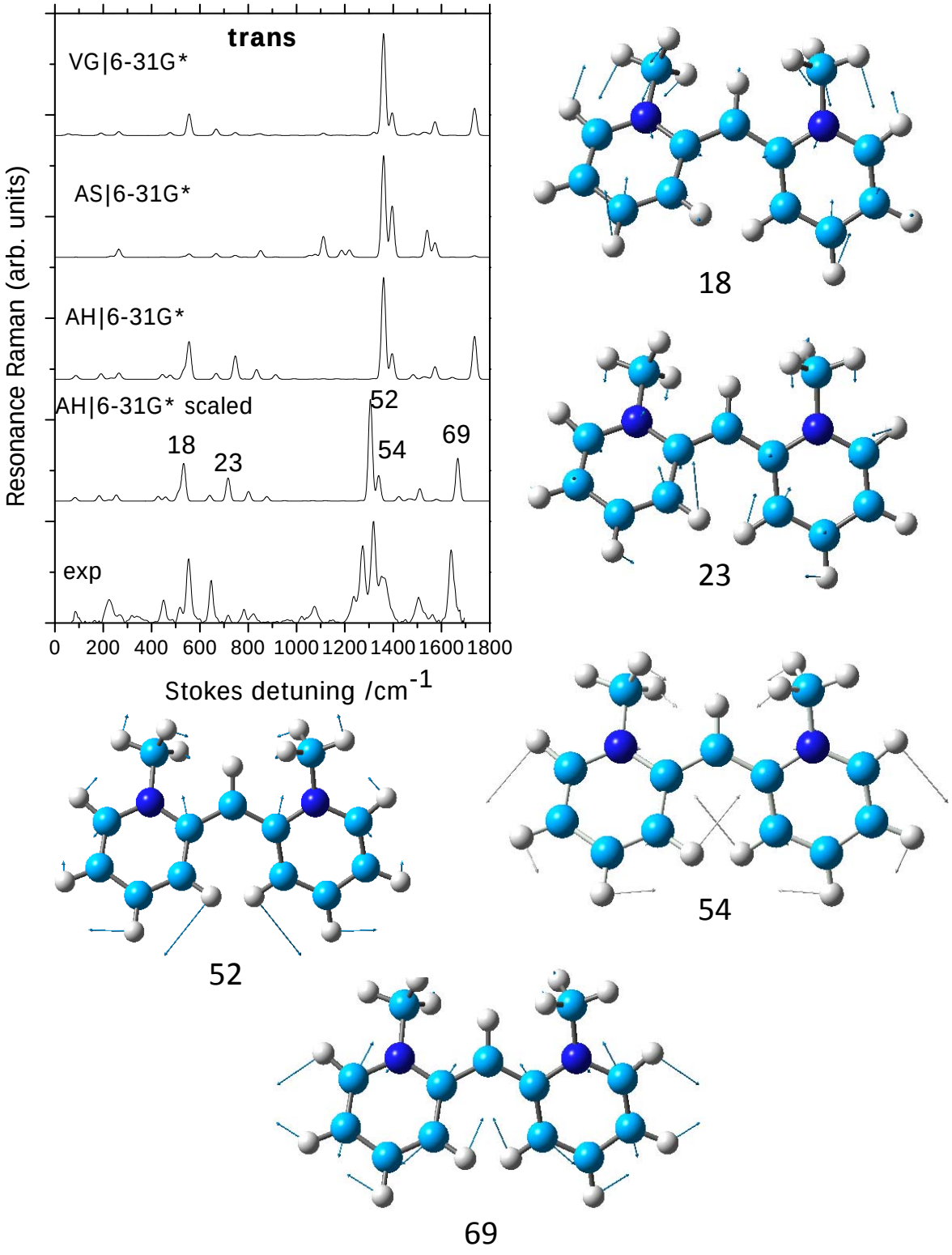

Fig. S6 Franck-Condon VG vibrational Raman spectra in resonance with the $S_0 \rightarrow S_1$ transition of the *trans* isomer of Me-P. The main bands are fundamental transitions of the sketched modes.

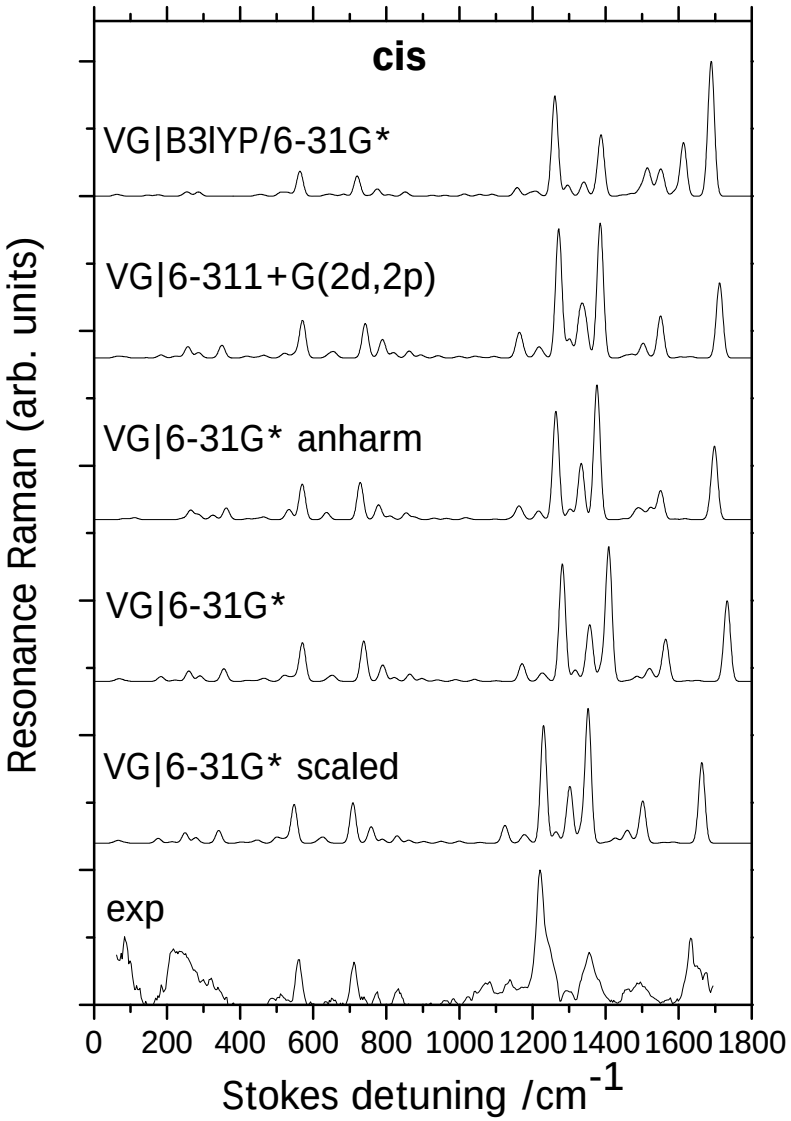

Fig. S7 Franck-Condon VG vibrational Raman spectra in resonance with the $S_0 \rightarrow S_1$ transition of the *cis* isomer of Me- , computed at different level of electronic theory. When not stated differently the CAM-B3LYP functional has been applied. "Scaled" indicates that calculated harmonic CAM-B3LYP/6-31G* frequencies have been multiplied by 0.96. Both anharmonic corrections and frequency scaling were applied by simply shifting the bands (leaving intensities unaffected).

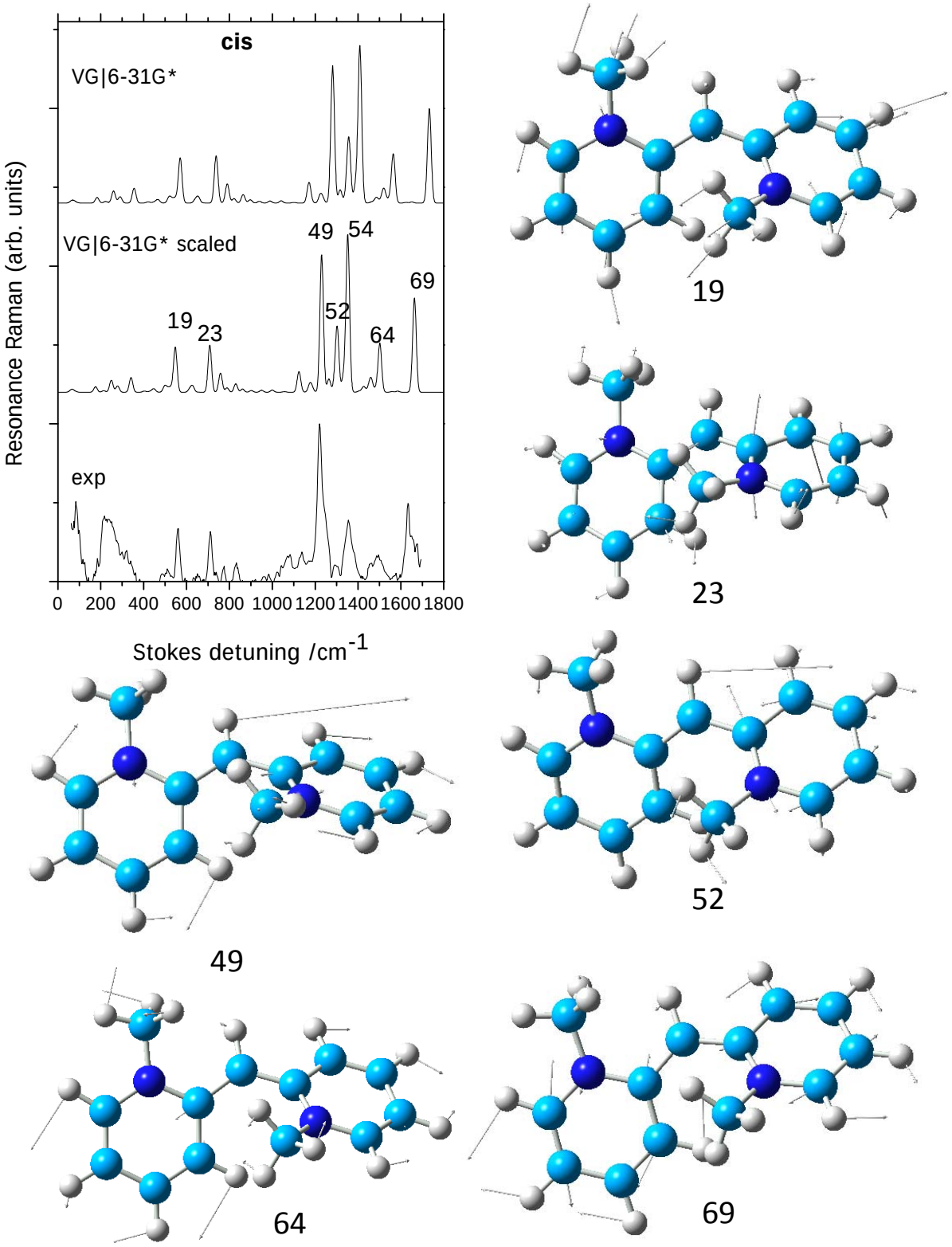

Fig. S8 Franck-Condon VG vibrational Raman spectra in resonance with the $S_0 \rightarrow S_1$ transition of the *cis* isomer of Me-1122-P. The main bands are fundamental transitions of the sketched modes

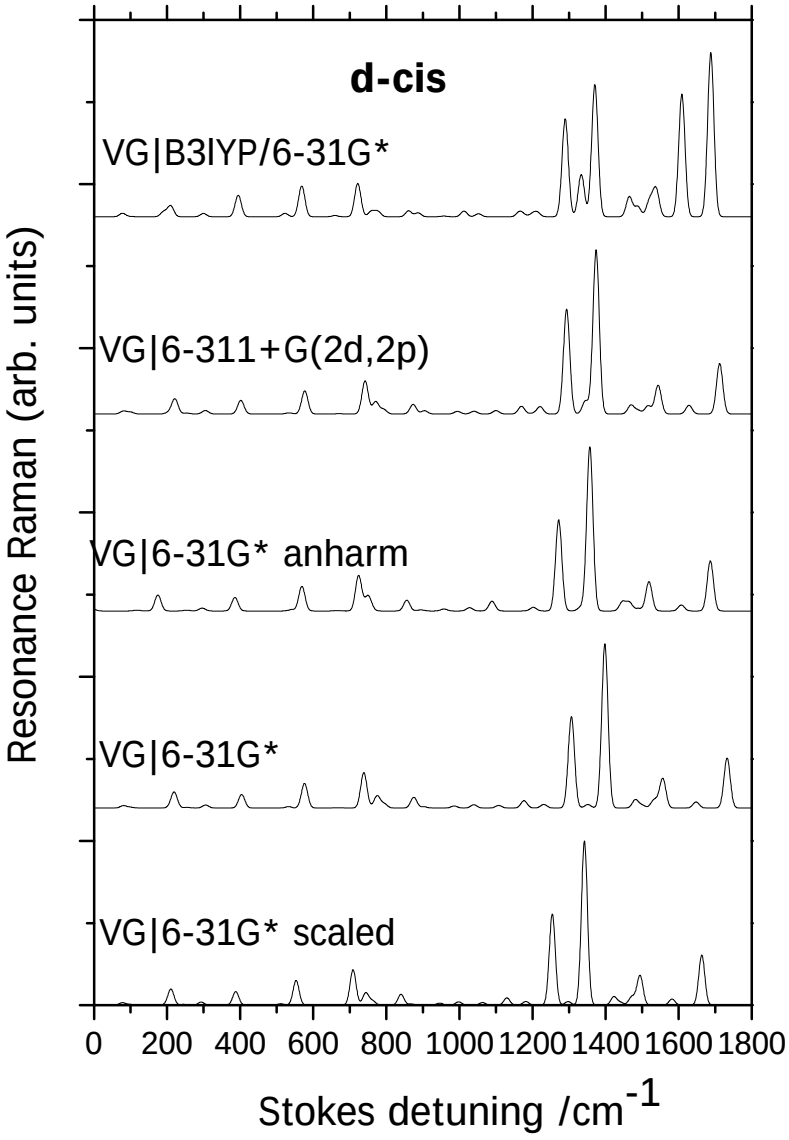

Fig. S9 Franck-Condon VG vibrational Raman spectra in resonance with the $S_0 \rightarrow S_1$ transition of the double-*cis* isomer of Me-1122-P, computed at different level of electronic theory. Conditions and labelling as in **Fig. S7**.

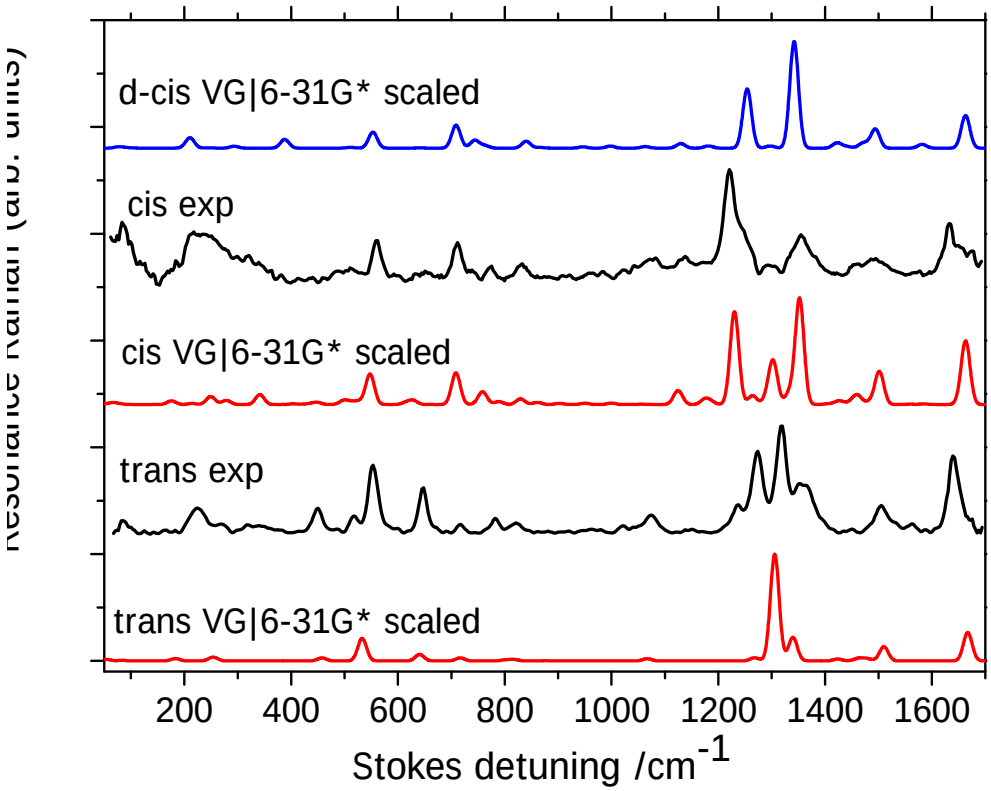

Fig. S10 Raman spectra in resonance with the $S_0 \rightarrow S_1$ transition: comparison of experimental SAS spectra with Franck-Condon VG vibrational Raman spectra. The latter were computed for the *trans*, *cis* and *dcis* isomers of Me-1122-P at harmonic CAM-B3LYP/6-31G* level, and harmonic frequencies have been multiplied by 0.96**.**

4.3 Assignments: mapping experimental transients to regions of the minimum energy path.

4.3.1 Simulation of the spectral evolution

$V_i^{(X)}(\psi)$ denotes the potential energy of state i, calculated for a fixed angle ψ, and with all other nuclear coordinates relaxed in state X. In formulas, angles are assumed to be measured in radian. But for visualisation, specific values will also be reported in degrees.

The starting distribution $P_{t=0}(\psi = \phi)$ is prepared in the electronic ground state. For the symmetrical state minS_0-*trans*, we calculate a frequency $\tilde{\nu}_{\text{torsion}} = 55\,\text{cm}^{-1}$ for the normal mode which comes closest to the conrotatory motion $\Delta\phi = \Delta\psi$. The moment-of-inertia for this torsional motion is estimated to be $m = 133.9$ amu Å^2. Thus we have

$$\frac{1}{hc} V_0^{(S0)}(\psi)/\text{cm}^{-1} = \frac{1}{2} 3003.6\,(\psi - 0.386)^2 . \qquad (1)$$

Assuming a temperature of 300 K, the corresponding Boltzmann distribution $P_{t=0}(\psi = \varphi)$ is centered at 22.1° and has FWHM of 17.8° (see **Fig. 7b**).

After electronic excitation, evolution along the C_2 path (see text) leads to minS_1-*trans* which has ϕ=ψ=29.7°. From here the C_1 path is assumed until minS_1 is reached at ψ=86.1° (where ϕ=2.1°). The composite potential energy curve is described as follows:

$$\frac{1}{hc} V_1^{(S1)}(\psi)/\text{cm}^{-1} = \frac{1}{2}(U_A + U_B) - \frac{1}{2}\sqrt{(U_A - U_B)^2 + 4w^2} \qquad (2)$$

$$U_A = \frac{1}{2} k_A (\psi - \psi_A)^2 + g_A \quad \text{and} \quad U_B = \frac{1}{2} k_B (\psi - \psi_A)^2 + g_B \qquad (3)$$

where $\psi_A = 0.4701,\ k_A = 26099,\ g_A = 25458$ and $\psi_B = 1.559,\ k_B = 6807,\ g_B = 23151,$ with w=974.

Seen from the composite path mentioned above, the potential energy $V_0^{(S1)}(\psi)$ of the ground state is described by Eqs. 2 and 3 but with the following parameters: $\psi'_A = 0.391,\ k'_A = 37699,\ g'_A = 1282,$ and $\psi'_B = 1.258,\ k'_B = 3374,\ g'_B = 6215,$ with $w' = 696$.

The oscillator strength for emission, $f(\psi)$ (**Fig. 7a**) is here given for regularly-spaced ψ values:

Ψ	0.0	0.1	0.2	0.3	0.4	0.5	0.6	0.7	0.8	0.9	1.0	1.1	1.2	1.3	1.4	1.5
f:	0.730	0.718	0.703	0.682	0.658	0.625	0.585	0.454	0.226	0.137	0.078	0.043	0.027	0.016	0.008	0.006

The Smoluchowski-equation governs diffusional motion of a distribution P_t as follows

$$\dot{P} = -\mathfrak{S}\ P \tag{4}$$

with the Smoluchowski-Operator[21]

$$\mathfrak{S} = -\frac{1}{\gamma m}\left\{k_B T\frac{\partial^2}{\partial q^2} + \left(\frac{\partial V}{\partial q}\right)\frac{\partial}{\partial q} + \left(\frac{\partial^2 V}{\partial q^2}\right)\right\} \tag{5}$$

Here γ is the friction rate constant [s^{-1}] and m the effective mass. In the current case of torsional motion, the dynamical coordinate $q \equiv \psi$ [rad] and therefore $m \equiv$ moment-of-inertia. For the minS_1-*trans* structure, m corresponds to 139.02 amu Å^2. The potential energy becomes $V(q) \equiv V_1^{S1}(\psi)$ from above. Furthermore T=300 K is assumed also for the evolution in S_1. We find below that γ=4.42 ps^{-1} describes best the observed decay and shift of the emission spectrum (**Fig. 3a**).

For numerical solutions we consider the range $q_{min} = -0.5....q_{max} = +2.25$ and use a virtual harmonic oscillator. This allows to cast all operators into matrix form. A basis set of n=200 vibrational wavefunctions is centered in the range, and the n^{th} virtual vibrational state is adjusted to have classical turning points at q_{min}, q_{max}. The coordinate q and the spatial derivative $\partial/\partial q$ are each represented by a band matrix. At the eigenvalues q_i the potential is sampled, and with this V can be represented conveniently.[22] Note that $\mathfrak{S}$ is non-normal because of the second term in eq. (5). Consequently its eigenvectors are not orthonormal. Even though, they may be used to express the general propagator $\exp\{-\mathfrak{S}\,t\}$. If this $n \times n$ matrix is applied to the expansion coefficients of $P_{t=0}(q)$, then the coefficients of $P_t(q)$ are obtained.

References

[1] P. Murril, *J. Amer. Chem. Soc.*, 1899, **21**, 828

[2] F. M. Hamer, M. I. Kelly, *J. Chem. Soc.*, 1931, 777

[3] L. G. S. Brooker, G.H. Keyes, *J. Amer. Chem. Soc.* 1935, **57**, 2488

[4] H. J.; Friedrich, W.; Gückel, G. Scheibe, *Chem. Ber.*, 1962, **95**, 1378

[5] I. Leubner, J. Dehler, G. Hohlneicher, *Ber. Bunsenges. Phys. Chem.*, 1967, **71**, 560

[6] G. S. Levinson, W. T. Simpson, W. Curtis, *J. Amer. Chem. Soc.* 1957, **79**, 4314

[7] G. Scheibe, E. Daltrozzo, O. Wörz, *Z. Phys. Chem.,* 1969, **64**, 97

[8] J. Tomasi, B. Mennucci, R. Cammi, *Chem. Rev.* 2005, **105**, 2999

[9] G. Scalmani, M. J. Frisch, B. Mennucci, J. Tomasi, R. Cammi, V. Barone, *J. Chem. Phys.* 2006, **124**, 094107.

[10] V. Barone, R. Improta, N. Rega, *Acc. Chem. Res.* 2008, **41**, 605

[11] F. Santoro, R. Improta, A. Lami, J. Bloino, V. Barone, *J. Chem. Phys.* 2007, **126**, 084509.

[12] F. Santoro, A. Lami, R. Improta, V. Barone, *J. Chem. Phys.* 2007, **126**, 184102

[13] R. Improta, V. Barone, G. Scalmani, M. J. Frisch, *J. Chem. Phys.* 2006, **125**, 054103.

[14] R. Improta, M. J. Frisch, G. Scalmani, V. Barone, *J. Chem. Phys.* 2007, **127**, 74504.

[15] R. Improta, F. Santoro, *J. Chem. Theory Comput*. 2005, **1**, 215

[16] D. Jacquemin, V. Wathelet, E. A. Perpète, C. Adamo *J. Chem. Theor. Comput*. 2009, **5**, 2420

[17] D. Jacquemin, Y. Zhao,; R. Valero, C. Adamo, I. Ciofini, D. G. Truhlar, *J. Chem. Theory Comput*. DOI: 10.1021/ct200721d 2012

[18] P. Nuernberger, G. Vogt, G. Gerber, R. Improta, F. Santoro, *J. Chem. Phys.* 2006, **125**, 044512

[19] G. Vogt, P. Nuernberger, G. Gerber, R. Improta, F. Santoro, *J. Chem. Phys.* 2006, **125**, 044513

[20] D. Jacquemin, E. A. Perpète, G. Scalmani, M. J. Frisch, R. Kobayashi, C. Adamo *J. Chem. Phys.* 2007, **126**, 144105

[21] H. Risken, *The Fokker-Planck-Equation*, 2nd edition, Springer, Berlin 1989

[22] Z. Bacic, J.C. Light, *J. Chem. Phys*. 1986, **85**, 4597